HHS Public Access

Author manuscript

J Thromb Haemost. Author manuscript; available in PMC 2018 October 01.

Published in final edited form as:

J Thromb Haemost. 2017 October ; 15(10): 2005–2016. doi:10.1111/jth.13788.

Lipid Specificity of the Membrane Binding Domain of Coagulation Factor X

Melanie P. Muller[1,2,3], **Yan Wang**[2], **James H. Morrissey**[2], and **Emad Tajkhorshid**[1,2,3,*]

[1]Beckman Institute for Advanced Science and Technology, University of Illinois at Urbana-Champaign, Urbana, Illinois 61801, U.S.A

[2]Department of Biochemistry, University of Illinois at Urbana-Champaign, Urbana, Illinois 61801, U.S.A

[3]Center for Biophysics and Computational Biology, University of Illinois at Urbana-Champaign, Urbana, Illinois 61801, U.S.A

Summary

Background—Factor X (FX) binds to cell membranes in a highly phospholipid-dependent manner and, in complex with tissue factor and factor VIIa (FVIIa), initiates the clotting cascade. Experimental information concerning the membrane-bound structure of FX with atomic resolution has remained elusive due to the fluid nature of cellular membranes. FX is known to bind preferentially to phosphatidylserine (PS).

Objectives—To develop the first membrane-bound model of FX-GLA domain to PS at atomic level, and to identify PS-specific binding sites of FX-GLA domain.

Methods—MD simulations were performed to develop an atomic-level model for the FX-GLA domain bound to PS bilayers. We utilized a membrane representation with enhanced lipid mobility, termed highly mobile membrane mimetic (HMMM), permitting spontaneous membrane binding and insertion by FX-GLA in multiple 100-ns simulations. In 14 independent simulations, FX-GLA bound spontaneously to the membrane. The resulting membrane-bound models were converted from HMMM to conventional membrane and simulated for an additional 100 ns.

Results—The final membrane-bound FX-GLA model allowed for detailed characterization of the orientation, insertion depth, and lipid interactions of the domain, providing insight into the molecular basis of its PS specificity. All binding simulations converged to the same configuration despite differing initial orientations.

[*]To whom correspondence should be addressed: emad@life.illinois.edu; phone, +1-217-244-6914.
DR JAMES H MORRISSEY (Orcid ID : 0000-0002-1570-1569)
DR EMAD TAJKHORSHID (Orcid ID : 0000-0001-8434-1010)

Addendum

M. P. Muller, J. H. Morrissey and E. Tajkhorshid were responsible for study conception and design. M. P. Muller implemented the study, analyzed and interpreted the results, and drafted the manuscript. Y. Wang, J. H. Morrissey, and E. Tajkhorshid critically revised the manuscript for important intellectual content. All authors gave final approval of the manuscript to be published.

Disclosure

J. H. Morrissey reports support from Diagnostica Stago outside the submitted work.

Conclusions—Analysis of interactions between residues in FX-GLA and lipid charged groups allowed for potential PS specific binding sites to be identified. This new structural and dynamic information provides an additional step towards a full understanding of the role of atomic-level lipid-protein interactions in regulating the critical and complex clotting cascade.

Keywords

Factor X; molecular dynamics simulation; molecular models; phosphatidylserine; membrane proteins

Introduction

The coagulation cascade is a critical pathway triggered by vascular damage, terminating in the formation of a blood clot [1, 2]. Coagulation is extensively regulated through membrane interactions; the cascade is greatly accelerated upon binding of coagulation factors to negatively charged lipids of the membrane [3, 4]. Once bound, coagulation proteases become thousands of times more active [3, 5], metamorphosing from extremely poor to highly effective enzymes.

While membrane interactions play an important role in the coagulation cascade, the atomic-level details through which this regulation takes place are not yet fully elucidated [6–8]. Factor X (FX) is a serine protease zymogen in the final common pathway of coagulation, and must be activated to generate the “explosive” thrombin burst necessary for clotting [1, 3, 9–11]. Formation of complexes which include FX are highly membrane dependent [10]. FX is one of several coagulation proteins equipped with a specialized membrane-binding “GLA” domain. These proteins are collectively known as vitamin-K dependent proteins [3, 12, 13], as this vitamin is required for post-translational modification of multiple glutamates into γ-carboxyglutamic acid (GLA) residues, necessary for proper folding and activity of GLA domains [14]. Specific sites on GLA domains are also involved in complex formation between coagulation proteins [15, 16].

Each GLA residue carries a •2 charge, and typically coordinates one or more Ca^{2+} (or, sometimes, Mg^{2+}) ions [17, 18]. These ions are necessary for proper GLA domain folding, resulting in a motif where divalent metal ions and highly charged protein residues are packed into the protein’s center, while three hydrophobic residues in the ω-loop are exposed on the exterior [8, 19–24] (Figure 1). Upon membrane binding, hydrophobic ω-loop residues, which we term the “keel,” penetrate into the hydrophobic core of the membrane (Figure 1) [25, 26]. The bovine FX-GLA domain (PDB entry 1IOD [27]), illustrated in Figure 1, contains 8 Ca^{2+} ions and 11 GLA residues, mostly located close to the keel. Previous computational work on a similar domain, FVII-GLA, found that this region interacts with the charged headgroups of membrane phospholipids [25].

Despite high structural and sequence conservation [13], GLA domains from different coagulation factors show marked variance in lipid specificity and membrane binding affinity [3, 7, 28]. FX and most other vitamin K-dependent clotting proteins bind preferentially to phosphatidylserine (PS), while GLA domains of the closely related FVII and protein C bind preferentially to phosphatidic acid (PA) [28, 29]. While the PA headgroup consists of a

phosphate group alone, the PS headgroup includes three charged groups: a phosphate, a carboxyl, and an amino group.

Understanding the role of specific phospholipids in membrane binding of the FX GLA domain (FX-GLA) will greatly add to our knowledge of key elements in the coagulation cascade. Experimental efforts to acquire this knowledge have been hampered by the difficulty inherent to studying membrane-bound coagulation proteins at sufficiently high resolution to elucidate sources of lipid specificity [30, 31]. Previous computational studies of FX structure and dynamics did not include membrane interactions [11, 32].

Only one well-folded structure of FX-GLA has been experimentally characterized with all Ca^{2+} ions resolved, a bovine FX-GLA bound to a snake venom protein (PDB 1IOD). [27, 33] This structure was characterized in solution, and thus can give little insight into membrane binding. All structures characterized for human FX either lack the GLA domain or, when the GLA is resolved, show disordered protein folds and missing/unresolved Ca^{2+} ions [34]. Given the importance of Ca^{2+} ions in mediating membrane binding [25], it is unwise to draw conclusions on membrane binding from such structures.

All-atom MD simulations studying GLA domains have been impeded previously by the slow time-scales required to capture full membrane binding of the protein and to sufficiently sample equilibrium protein-lipid interactions [30]. In traditional membrane representations, slow diffusion of lipids–on the order of 10^{-8} cm^2 s^{-1} [31]–makes membrane binding and partial membrane insertion of peripheral membrane proteins such as GLA domains challenging if not impossible under currently achievable time scales. A reduced, yet atomistic, membrane representation, the highly mobile membrane mimetic (HMMM) [31], has been specifically designed to address this issue, allowing for faster lipid diffusion and thus, enhanced characterization of protein-lipid interactions at an atomic level. HMMM properties have been well characterized [31] and it has been applied with success to a variety of peripheral membrane protein systems [35–41], including characterizing a membrane-bound model of FVII-GLA [31].

Here, for the first time, we develop a model of membrane-bound FX-GLA using extensive molecular dynamics (MD) simulations using HMMM membranes to investigate protein-lipid interactions between FX-GLA and PS lipids. Starting from the solution crystal structure (PDB 1IOD [27]), we capture spontaneous binding of FX-GLA to a PS HMMM in 14 independent, unbiased simulations. Membrane-bound states are then converted to full-membrane representations. Results of 200 ns for each of the 14 FX-GLA structures reported here are used to characterize membrane penetration depth and membrane orientation of FX-GLA. Further, extensive sampling of lipid-protein interactions has allowed for detailed analysis of GLA-lipid interaction patterns and identification of putative PS-specific binding sites.

Methods

Membrane Binding Simulations

A crystal structure of bovine FX-GLA (which we will refer to hereafter as FX-GLA) from Protein Data Bank entry 1IOD [27] was used as the starting structure for our simulations. Using the PSFGEN plugin of VMD [42], an N-terminal ammonium group and a C-terminal N-methyl amide group were added, along with hydrogen atoms. The N-methyl amide group was chosen rather than a charged C-terminus because the C-terminus in the full length protein would be connected to the first FX epidermal growth factor (EGF1) domain, and a C-terminus with default charge would introduce an artificial charged group to this region. FX-GLA was next placed in a 60×60×60 $Å^3$ water box using the SOLVATE plugin of VMD. This box was neutralized with K^+ ions added using the AUTOIONIZE plugin of VMD and equilibrated for 1 ns after 2,000 steps of energy minimization. This solvated model was used as the starting point for all subsequent membrane-binding simulations.

Our HMMM membrane construct was used in binding simulations to allow for both increased lipid interaction sampling and ease of FX-GLA insertion. A detailed description of the HMMM can be found in Supplemental Material (Figure S1). We used a 100% PS membrane, although this deviates from the PS concentration in mammalian cells, to achieve enhanced sampling of FX-GLA interaction with this critical lipid. A 50×50×114 $Å^3$ solvated HMMM-PS lipid patch was constructed using the HMMM Builder in CHARMM-GUI [43]. Nine independent orientations were generated by placing FX-GLA 3 Å above the membrane, where 3 Å is the minimum distance between any GLA domain atom and any PS-membrane atom. Each FX-GLA membrane orientation was at least a rotation of 15° different in the x-z or y-z plane from every other orientation. Finally, each of the nine independent systems was neutralized with K^+ ions using the AUTOIONIZE plugin of VMD. We chose not to include free Ca^{2+} due to the very slow equilibration of free Ca^{2+} interactions with lipids. This is one of the limitations of the present study, as Ca^{2+} ions can potentially affect the electrostatic properties and structure of PS lipids. The final systems were each approximately 24,000 atoms. The z-position of HMMM short-tailed lipids was restrained harmonically (k=0.1 kcal/mol/$Å^2$ applied to lipid tail atoms with CHARMM force field numbers C31 and C21) throughout the simulations to more closely reproduce the natural distribution of head-group positions. Each of 9 independent FX-GLA systems was simulated 3 times with different initial velocities for a total of 27 independent simulations of 100 ns each (Figure 2).

Conversion of HMMM model to Conventional Membrane

To ensure the final FX-GLA membrane-bound model was not unduly affected by use of the HMMM as opposed to a full-tailed lipid construct, bound systems were converted to full-membrane, using a PDB generated from the final frame of each 100 ns HMMM simulation. Conversion to full-tailed membrane was only made for FX-GLA structures in which keel residues penetrated below the level of phosphates in the membrane, which we will hereafter refer to as “properly bound.” A total of 14 FX-GLA HMMM binding trajectories satisfied this criterion (Figure 2).

For conversion to full membranes, first the layer of 1,1-dicholoroethane (DCLE) solvent molecules was removed from the center of the HMMM bilayer. Then, a full-tailed lipid 1-palmitoyl-2-oleoyl-sn-glycero-3-phospho-L-serine (POPS), was overlaid onto each short-tailed lipid, and coordinates of missing atoms were copied from the full-tailed lipid, thus allowing for head-group interactions obtained from HMMM simulations to be preserved. In some cases, introduction of full lipids resulted in clashes between adjacent lipid tails. A 2,500-step energy minimization resolved such clashes. In a solitary case where three lipid tails overlapped at the same point, atoms of the overlapped tails were manually moved using VMD prior to the minimization step, eliminating the overlap. Each FX-GLA full-membrane system was simulated for another 100 ns.

Simulation Protocols

All simulations were performed using NAMD2 [44] and CHARMM36 [45] force-field parameters. Parameters of GLA residues were those previously developed by our lab [25] with atom-types renamed as appropriate for conversion from CHARMM27. The TIP3P water model was used for all simulations. Constant pressure was maintained at a target of 1 atm using the Nosé-Hoover-Langevin piston method [46]. Constant temperature was maintained by Langevin dynamics with a damping coefficient, γ, of 1 ps^{-1} applied to all atoms [47]. All simulations used a 2 fs time step and a temperature of 310 K. Covalent bonds involving hydrogens and the H-O-H angle were fixed using the SHAKE and RATTLE algorithms [48, 49]. The particle mesh Ewald (PME) method [50] was used for long-range electrostatic calculations with a grid density greater than $1/Å^3$. Non-bonded interactions were truncated after 12 Å with a smoothing function starting at 10 Å. System setup, visualization, and analysis were carried out using VMD [42].

Analysis

Depth of GLA domain insertion into the membrane was assessed by calculating the z component of the center of mass (COM) of backbone atoms in residues PHE4, LEU5, and VAL8 in the FX-GLA keel relative to the average plane of the phosphate groups (phosphorous atoms and four bonded oxygen atoms) of PS lipids. The z-position of COM of Ca^{2+} ions 1–7 (Ca-1 to Ca-7), z-position of COM of the lipid carboxyl groups (carbon and two bonded oxygen atoms), and z-position of COM of amino groups (nitrogen and three bonded hydrogen atoms) were also calculated relative to the phosphate plane (Figure 3); from this point forward the terms Ca^{2+} ions, phosphate, carboxyl and amino groups will refer to the atoms specified above.

Orientation of FX-GLA relative to the membrane plane was assessed using two angles defined in perpendicular planes, termed “port-to-starboard” and “bow-to-stern” (see Figure 1 for locations on GLA domain of port, starboard, bow and stern). The bow-to-stern angle is the angle between the membrane normal (z-axis) and the vector connecting the COMs of Ca-1,2,3 and Ca-4,5,6 (see Figure 4). The port-to-starboard angle is the angle between the membrane normal and the vector connecting COM of backbone atoms in LEU13, GLA14, GLA29, and VAL30 and COM of backbone atoms in GLA19, CYS22, SER23 and LEU24. These two sets of residues represent opposite ends of the two helices directly above the level of the coordinated Ca^{2+} ions. Thus, the bow-to-stern angle represents relative tilt of the stern

and bow ends of FX-GLA to the membrane normal, while the port-to-starboard angle represents relative tilt of the port and starboard ends relative to the membrane normal.

Contacts between lipid headgroup charged moieties and FX-GLA (bound Ca^{2+} or protein residues) were calculated based on specific distance cutoffs which were determined using radial pair distribution function calculations. Number of contacts here is pairs of atoms within a specified cutoff distance. Distance between all protein and Ca^{2+} atoms and phosphate, amino, and carboxyl atoms were calculated. Radial pair distribution functional analysis was performed separately for distances between the residue type of interest (protein or Ca^{2+} ions) and the lipid head-group moiety of interest (carboxyl, amino, or phosphate).

The contacts calculations sampled every 20 ps of the 100 ns full-membrane simulation. For protein residues and Ca^{2+} ions, all atoms were included in the contact number calculation. Cutoffs determined were 2.50 Å for phosphate-Ca^{2+}, 3.00 Å for carboxyl-Ca^{2+}, 2.25 Å for phosphate-protein, 2.50 Å for carboxyl-protein, and 2.25 Å for amino-protein contacts. See Figure S2 in Supplemental Material for the radial distribution functions. To ensure all atoms interacting with protein were included in the calculation, the periodic box was centered around the protein and all atoms wrapped into the same periodic box.

To screen for putative PS-specific binding interactions, average number of protein and Ca^{2+} contacts per lipid were calculated for full-membrane simulations. Lipids with high average protein contacts were visually inspected to determine whether more than one charged group on the lipid was interacting simultaneously with FX-GLA.

Number of water molecules in the interfacial region was quantified by measuring number of molecules both within 2 Å of GLA residues (protein or calcium) and 2 Å of PS. Data was smoothed using a Gaussian running average with averaging over 50 ps intervals (S5 in supplemental material).

Results and Discussion

Spontaneous Membrane Insertion of the FX-GLA Domain

To characterize the membrane-bound configuration of FX-GLA, we performed membrane-binding simulations starting with 27 copies of FX-GLA in 9 independent orientations and placed above a 100% PS HMMM membrane. After 100 ns, 14 of 27 FX-GLAs were observed to insert keel residues spontaneously into the membrane (Figure 3). Following keel insertion (positioning below the lipid phosphate plane), each FX-GLA quickly established a stable binding pose which is conserved across all 14 FX-GLAs. As shown in Figure 3, after the keel crosses the charged layer of lipid headgroups, insertion depth of both keel residues and Ca^{2+} ions converge within 10 ns. For equilibrated trajectories, COM of keel residues reaches a depth of 5 Å below the lipid phosphate plane, penetrating well into the membrane's hydrophobic core. COM of Ca^{2+} ion converges to a z-position 2 Å or less above of the carboxyl plane, and approximately 5 Å above the phosphate plane. Similarly, the 14 FX-GLAs, despite highly varied initial orientations, converged to similar port-to-starboard and bow-to-stern orientations relative to the membrane subsequent to keel insertion (Figure 4). A well-defined binding pose can thus be characterized using these 14 trajectories in

terms of both depth of insertion and orientation. The remaining FX-GLA simulations failed to insert keels into the hydrophobic core during 100 ns HMMM simulations (11 simulations), or showed GLA domain fold instability (2 simulations), and thus were not included in further analysis (Figure S3 in Supplemental Material). Number of water molecules in the interfacial region were quantified, and this analysis can be found in Figure S5 in Supplemental Material.

The 14 properly bound FX-GLA models were converted from HMMM to a conventional membrane representation. Both orientation relative to and insertion depth within the membrane plane was stable in 100 ns of simulation following membrane conversion (Figures 3 and 4). Indeed, membrane binding depth and orientation among the 14 trajectories further converges during the conventional membrane simulations. Distribution of bow-to-stern angles (Figure 4C, upper panel) follows a classic normal distribution centered at 85°, suggesting FX-GLA is either parallel to the membrane or tilted slightly toward the bow. Distribution of port-to-starboard angles is less regular, with the majority of angles lying between 90–120° and a small population at about 65°. This indicates that in most bound FX-GLAs the starboard end of the protein is tilted towards the membrane at about 10°, potentially enabling the GLA32 residue to interact with lipids (Figure 1).

Fluctuations in binding height and orientation were found, as expected, to decrease upon conversion to a full-membrane representation. This is consistent with lessened perturbation of the binding pose through slower lateral diffusion of surrounding lipids. Our membrane-bound FX-GLA model is thus stable under normal membrane conditions, and shows minimal perturbation upon shifting from HMMM to conventional membrane.

PS Specific Binding of the FX-GLA Domain

Protein-lipid interactions were analyzed using all 100-ns trajectories obtained from full-membrane simulations to provide information on the nature of PS interactions with FX-GLA, as well as the location and characteristics of putative PS-specific binding sites. FX is highly PS specific, even stereochemically specific [51], while other closely related GLA domains (FVII, protein C) are specific to other anionic lipids [28, 29, 51]. It is unknown how atomic-level interactions give rise to this specificity. Given the importance of PS interactions in FX binding, we examined all contacts between FX-GLA residues and each of the PS charged groups, namely phosphate (−1), carboxyl (−1), and amino (+1) groups.

Examination of protein-lipid contacts reveals an interesting pattern (Figure 5). The significant amino group contacts (average contact number greater than 0.2) occur with specialized GLA residues. All but one of the GLA residues show significant interactions with lipid amino groups, meeting the cutoff distance criterion in 25–40% of all trajectory frames with low standard deviations. This indicates that at any given time, approximately two GLA residues interact with lipid amino groups. GLA7, which has backbone atoms in the ω-loop, is most likely to be engaged in this interaction (0.45 average contact number), while GLA residues in the two helices located above the level of Ca^{2+} ions 1–7 (residues 13 to 32) have approximately equal likelihood of interacting with a lipid amino group (•0.3 average contact number) (Figure 5, Table 1). GLA32 shows significant lipid amino

interactions, consistent with the observation that the starboard end of FX-GLA generally tilts toward the membrane.

The majority of contacts between Ca^{2+} ions and lipids are with the lipid carboxyl groups; at any given time there is at least one lipid carboxyl group bound to each of the bow Ca^{2+} ions (Ca-1 and Ca-2) and stern Ca^{2+} ions (Ca-6 and Ca-7). Ca-6 also frequently interacts with lipid phosphate (0.52 average contact number) (Figure 5, Table 2). Three center Ca^{2+} ions (Ca-3, Ca-4, and Ca-5) show no contacts with lipid charged groups, indicating their primary role in structural stability of the GLA domain [25]. Ca^{2+} ions which interact with PS carboxyl groups are all coordinated by GLA residues with significant lipid amino group interactions. This suggests the same PS lipid may contribute carboxyl and amino groups for both interactions.

The primary lipid-phosphate binding sites on FX-GLA consist of two clusters of residues on the port and starboard faces of the protein, with the cluster consisting of LYS9, GLN10, and ARG15 on the starboard side (0.50, 0.43, and 0.37 average contact number, respectively) being particularly consistent and prominent throughout the trajectories. As shown in Figure 5B, the side chains of these residues have a very similar z-position relative to the keel and are located on the starboard side of the protein, forming a lipid phosphate binding patch. SER3 and ASN2 on the port side (with 0.16 and 0.27 average contact numbers, respectively) can also anchor the GLA in the membrane through lipid phosphate binding, but this is observed less frequently than binding to the port cluster. The overall binding pattern for FX-GLA is tiered; charged residues close to the keel primarily form lipid phosphate contacts, while those surrounding the Ca^{2+} ions participate in interactions with lipid amino and, more rarely, lipid carboxyl charged groups (SER23, ARG28).

We identified a number of putative PS-specific binding sites, or sites where PS lipids bound using multiple charged groups. In some instances, all three functional groups on a PS lipid simultaneously engaged with protein residues and Ca^{2+} ions. Interactions with multiple charged groups on the same lipid are more likely indicative of PS-specific sites. The two putative PS-specific binding sites we consider most likely based on the performed contact analysis are shown in Figure 6. These are interactions between: 1) PS, GLA19, Ca-6 and Ca-7; 2) PS, GLA29, GLN10, and Ca-1 (Figure 6). Additional PS binding modes observed in our simulations are shown in Supplemental Material (Figure S4). Each mode of interaction reported in Figures 6 and S4 was stable for at least 50 ns in the full-membrane simulations. In the majority of cases, a PS carboxyl group interacts with a Ca^{2+} ion and the PS amino group interacts simultaneously with one of the GLA residues which coordinates that same Ca^{2+} ion.

Comparison to Other GLA Domains

Sources of marked differences in binding affinity for PS exhibited by coagulation factor GLA domains remain to be investigated. Clearly, specific FX-GLA residues actively engage all important PS charged groups. However, many of these residues are identical in other GLA domains which bind with lesser affinity to PS. For example, FVII-GLA, which shows low PS affinity [7], has a nearly identical GLA residue placement as FX in the portion of the domain which actively interacts with lipids. The sole exception is GLA32, the last of 44

residues in FX-GLA to interact with lipids according to our analysis, and which in FVII-GLA is LYS32 (Figure 7).

According to our analysis, dissimilar residues between the domains which are involved in PS charged-group interactions for FX-GLA are SER3, LYS9, GLN10, and GLA32. In FVII-GLA, these residues are ALA3, ARG9, PRO10, and LYS32. The location of these residues is highlighted in violet in Figure 7. The change from GLA to LYS at position 32 reverses the charge at that position, changing it from −2 to +1. Interestingly, FIX, known like FX to have high PS specificity [19], also has a GLA residue in this position, while protein C, which like FVII binds with high affinity to phosphatidic acid, [7] has a GLN residue. This residue would be a good target for mutational studies, as our analysis suggests it may be involved in PS-specific interactions but is not involved in structural coordination of Ca^{2+} ions.

The change of SER3 and GLN10 in FX to hydrophobic residues in FVII may change the pattern of phosphate-protein interactions, which could influence favorability of PS binding. Interestingly, one of the equivalent residues on the bovine prothrombin GLA domain (PT-GLA) was found in a previous experimental study [8] to bind PS. The lipid carboxyl group interacts with Ca^{2+} ions while the phosphate group binds to the charged patch formed by LYS3, ARG16, and ARG10 [8] (Figure 8). The PS pocket on PT-GLA is located in nearly the same position as the SER3, LYS9, GLN10, ARG15 phosphate binding patch found on our FX-GLA, although the SER3 side-chain is likely too short to participate with LYS9 and ARG16 in simultaneously binding a PS as in PT-GLA. It is possible these sites on various GLA domains form nonspecific phosphate binding patches involved in modulating protein orientation, and thus indirectly modulating lipid affinity and even FX activation rates.

Conclusions

In this study, we report the first structural model for the membrane-bound state of FX-GLA, the membrane-binding domain of a critical coagulation protein, and propose two putative PS-specific binding sites based on the simulation results. Experimental data showing binding of lysoPS to the prothrombin GLA-domain are consistent with our results [8], as the single lipid in this experiment bound with its phosphate group to a site identified on FX-GLA as a phosphate binding site. Further experimental studies of effects of mutating GLA32 and residues of the phosphate binding pocket will be informative as they can validate the proposed model of binding in this study. Mutation of additional GLA residues might also be useful if effected without modifying the FX-GLA fold and Ca^{2+} coordination. It is possible that GLA7 and GLA25 provide sufficient structural support to coordinate Ca^{2+} ions 1 and 2 without GLA29.

In order to enhance sampling of PS-GLA interactions, an artificially high PS concentration (100% PS) was used in combination with a membrane representation with enhanced lipid dynamics (HMMM). Provided sufficient computational power, future studies will examine the protein in a more native membrane environment, composed of a mixed lipid bilayer and taking into account the impact of bulk solution divalent ions such as Ca^{2+} and Mg^{2+}, thereby improving the realism of the environment and its relevance to physiological conditions.

Another natural extension of the present study is to employ models of human coagulation factors.

Despite these technical limitations, the structural model developed in the present study will serve as the first structural framework allowing for more rationally designed experiments investigating, e.g., the impact of specific mutations on the activity of FX, or develop small molecules for potential drug targets that would block lipid-specific binding of FX-GLA domains with the goal of diminishing thrombosis.

Supplementary Material

Refer to Web version on PubMed Central for supplementary material.

Acknowledgments

This work was supported by the National Institutes of Health (Grants R01-GM123455 to J. H. Morrissey and E. Tajkhorshid, and P41-GM104601and U54-GM087519 to E.T.), NCSA Blue Waters compute resources, and XSEDE compute resources (Grant TG-MCA06N060 to E. Tajkhorshid).

References

1. Davie EW, Fujikawa K, Kisiel W. The coagulation cascade: Initiation, maintenance, and regulation. Biochemistry. 1991; 30:10363–10370. [PubMed: 1931959]
2. Mann K, Nesheim M, Church W, Haley P, Krishnaswamy S. Surface-dependent reactions of the vitamin K-dependent enzyme complexes. Blood. 1990; 76:1–16. [PubMed: 2194585]
3. Zwaal RFA, Comfurius P, Bevers EM. Lipid-protein interactions in blood coagulation. Biochim Biophys Acta. 1998; 1376:433–453. [PubMed: 9805008]
4. Shaw AW, Pureza VS, Sligar SG, Morrissey JH. The local phospholipid environment modulates the activation of blood clotting. J Biol Chem. 2007; 282:6556–6563. [PubMed: 17200119]
5. Neuenschwander PF, Morrissey JH. Roles of the membrane-interactive regions of factor VIIa and tissue factor – the factor VIIa Gla domain is dispensable for binding to tissue factor but important for activation of factor X. J Biol Chem. 1994; 269:8007–8013. [PubMed: 8132522]
6. McDonald JF, Shah AM, Schwalbe RA, Kisiel W, Dahlbäck B, Nelsestuen GL. Comparison of naturally occurring vitamin K-dependent proteins: Correlation of amino acid sequences and membrane binding properties suggests a membrane contact site. Biochemistry. 1997; 36:5120–5127. [PubMed: 9136872]
7. Tavoosi N, Smith SA, Davis-Harrison RL, Morrissey JH. Factor VII and protein C are phosphatidic acid-binding proteins. Biochemistry. 2013; 52:5545–5552. [PubMed: 23879866]
8. Huang M, Rigby AC, Morelli X, Grant MA, Huang G, Furie B, Seaton B, Furie BC. Structural basis of membrane binding by Gla domains of vitamin K-dependent proteins. Nat Struct Biol. 2003; 10:751–756. [PubMed: 12923575]
9. Kamata K, Kawamoto H, Honma T, Iwama T, Kim SH. Structural basis for chemical inhibition of human blood coagulation factor Xa. Proc Natl Acad Sci USA. 1998; 95:6630–6635. [PubMed: 9618463]
10. Qureshi SH, Yang L, Manithody C, Rezaie AR. Membrane-dependent interaction of factor X and prothrombin with factor Va in the prothrombinase complex. Biochemistry. 2009; 48:5034–5041. [PubMed: 19378973]
11. Venkateswarlu D, Perera L, Darden T, Pedersen LG. Structure and dynamics of zymogen human blood coagulation factor X. Biophys J. 2002; 82:1190–1206. [PubMed: 11867437]
12. Furie B, Furie BC. The molecular basis of blood coagulation. Cell. 1988; 53:505–518. [PubMed: 3286010]

13. Nelsestuen G, Shah A, Harvey S. Vitamin K-dependent proteins. Vitam Horm. 2000; 58:355–389. [PubMed: 10668405]
14. Vermeer C. γ-carboxyglutamate-containing proteins and the vitamin K-dependent carboxylase. Biochem J. 1990; 266:625–636. [PubMed: 2183788]
15. Blostein MD, Rigby AC, Jacobs M, Furie B, Furie BC. The Gla domain of human prothrombin has a binding site for factor Va. J Biol Chem. 2000; 275:38120–38126. [PubMed: 10973980]
16. Huang Q, Neuenschwander PF, Rezaie AR, Morrissey JH. Substrate recognition by tissue factor-factor VIIa – evidence for interaction of residues Lys^{165} and Lys^{166} of tissue factor with the γ-carboxyglutamate-rich domain of factor X. J Biol Chem. 1996; 271:21752–21757. [PubMed: 8702971]
17. Tavoosi N, Morrissey JH. Influence of membrane composition on the enhancement of factor VII/tissue factor activity by magnesium ions. Thromb Haemost. 2014; 111:565–779. [PubMed: 24651947]
18. Vadival K, Agah S, Messer AS, Cascio D, Bajaj MS, Krishnaswamy S, Esmon CT, Padmanabhan K, Bajaj SP. Structural and functional studies of γ-carboxyglutamic acid domains of factor VIIa and activated protein C: role of magnesium at physiological calcium. J Mol Biol. 2013; 425:1961–1981. [PubMed: 23454357]
19. Stace CL, Ktistakis NT. Phosphatidic acid and phosphatidylserine-binding proteins. Biochim Biophys Acta. 2006; 1761:913–926. [PubMed: 16624617]
20. Freedman SJ, Furie BC, Furie B, Baleja JD. Structure of the metal-free γ-carboxyglutamic acid-rich membrane binding region of factor IX by two-dimensional NMR spectroscopy. J Biol Chem. 1995; 270:7980–7987. [PubMed: 7713897]
21. Freedman S, Furie B, Furie B, Baleja J. Structure of the calcium ion-bound γ-carboxyglutamic acid rich domain of factor IX. Biochemistry. 1995; 34:12126–12137. [PubMed: 7547952]
22. Soriano-García M, Padmanabhan K, de Vos AM, Tulinsky A. The Ca^{2+} ion and membrane binding structure of the GLA domain of Ca-prothrombin fragment 1. Biochemistry. 1992; 31:2554–2566. [PubMed: 1547238]
23. Sunnerhagen M, Forsén S, Hoffrén AM, Drakenberg T, Teleman O, Stenflo J. Structure of the Ca^{2+}-free GLA domain sheds light on membrane binding of blood coagulation proteins. Nat Struct Biol. 1995; 2:504–509. [PubMed: 7664114]
24. Park C, Tulinsky A. Three-dimensional structure of the kringle sequence: structure of prothrombin fragment 1. Biochemistry. 1995; 25:7980–7987.
25. Ohkubo YZ, Tajkhorshid E. Distinct structural and adhesive roles of Ca^{2+} in membrane binding of blood coagulation factors. Structure. 2008; 16:72–81. [PubMed: 18184585]
26. Falls LA, Furie BC, Jacobs M, Furie B, Rigby AC. The ω-loop region of the human prothrombin γ-carboxyglutamic acid domain penetrates anionic phospholipid membranes. J Biol Chem. 2001; 276:23895–23902. [PubMed: 11312259]
27. Mizuno H, Fujimoto Z, Atoda H, Morita T. Crystal structure of an anticoagulant protein in complex with the Gla domain of factor X. Proc Natl Acad Sci USA. 2001; 98:7230–7234. [PubMed: 11404471]
28. Tavoosi N, Davis-Harrison RL, Pogorelov TV, Ohkubo YZ, Arcario MJ, Clay MC, Rienstra CM, Tajkhorshid E, Morrissey JH. Molecular determinants of phospholipid synergy in blood clotting. J Biol Chem. 2011; 286:23247–23253. [PubMed: 21561861]
29. Krishnaswamy S, Field KA, Edgington TS, Morrissey JH, Mann KG. Role of the membrane surface in the activation of human coagulation factor X. J Biol Chem. 1992; 267:26110–267120. [PubMed: 1464622]
30. Morrissey JH, Tajkhorshid E, Rienstra CM. Nanoscale studies of protein-membrane interactions in blood clotting. J Thromb Haem. 2011; 9(Suppl 1):167–167.
31. Ohkubo YZ, Pogorelov TV, Arcario MJ, Christensen GA, Tajkhorshid E. Accelerating membrane insertion of peripheral proteins with a novel membrane mimetic model. Biophys J. 2012; 102:2130–2139. [PubMed: 22824277]
32. Venkateswarlu D, Duke R, Perera L, Darden TA, Pedersen LG. An all-atom solution-equilibrated model for human extrinsic blood coagulation complex (sTF-VIIa-Xa): a protein-protein docking and molecular dynamics refinement study. J Thromb Haem. 2003; 1:2577–2588.

33. Sunnerhagen M, Olah GA, Stenflo J, Forsén S, Drankenberg T, Trewhella J. The relative orientation of Gla and EGF domains in coagulation factor X is altered by Ca^{2+} binding to the first EGF domain. a combined NMR-small angle X-ray scattering study. Biochemistry. 1996; 35:11547–11559. [PubMed: 8794734]
34. Wang SX, Hur E, Sousa CA, Brinen L, Slivka EJ, Fletterick RJ. The extended interactions and Gla domain of blood coagulation factor Xa. Biochemistry. 2003; 42:7959–7966. [PubMed: 12834348]
35. Arcario MJ, Tajkhorshid E. Membrane-induced structural rearrangement and identification of a novel membrane anchor in Talin F2F3. Biophys J. 2014; 107:2059–2069. [PubMed: 25418091]
36. Madsen JJ, Ohkubo YZ, Peters GH, Faber JH, Tajkhorshid E, Olsen OH. Membrane interaction of the factor VIIIa discoidin domains in atomistic detail. Biochemistry. 2015; 54:6123–6131. [PubMed: 26346528]
37. Baylon JL, Lenov IL, Sligar SG, Tajkhorshid E. Characterizing the membrane-bound state of cytochrome P450 3A4: Structure, depth of insertion, and orientation. J Am Chem Soc. 2013; 135:8542–8551. [PubMed: 23697766]
38. Baylon JL, Vermaas JV, Muller MP, Arcario MJ, Pogorelov TV, Tajkhorshid E. Atomic-level description of protein-lipid interactions using an accelerated membrane model. Biochim Biophys Acta Biomembr. 2016; 1858:1573–1583.
39. Vermaas JV, Baylon JL, Arcario MJ, Muller MP, Wu Z, Pogorelov TV, Tajkhorshid E. Efficient exploration of membrane-associated phenomena at atomic resolution. J Membr Biol. 2015; 248:563–582. [PubMed: 25998378]
40. Vermaas JV, Tajkhorshid E. Conformational heterogeneity of α-synuclein in membrane. Biochim Biophys Acta Biomembr. 2014; 1838:3107–3117.
41. Baylon JL, Tajkhorshid E. Capturing spontaneous membrane insertion of the influenza virus hemagglutinin fusion peptide. J Phys Chem B. 2015; 119:7882–7893. [PubMed: 25996559]
42. Humphrey W, Dalke A, Schulten K. VMD – Visual Molecular Dynamics. J Mol Graphics. 1996; 14:33–38.
43. Qi Y, Cheng X, Lee J, Vermaas JV, Pogorelov TV, Tajkhorshid E, Park S, Klauda JB, Im W. CHARMM-GUI HMMM builder for membrane simulations with the highly mobile membrane-mimetic model. Biophys J. 2015; 109:2012–2022. [PubMed: 26588561]
44. Kalé L, Skeel R, Bhandarkar M, Brunner R, Gursoy A, Krawetz N, Phillips J, Shinozaki A, Varadarajan K, Schulten K. NAMD2: Greater scalability for parallel molecular dynamics. J Comp Phys. 1999; 151:283–312.
45. Klauda JB, Venable RM, Freites JA, O'Connor JW, Tobias DJ, Mondragon-Ramirez C, Vorobyov I, MacKerell AD Jr, Pastor RW. Update of the CHARMM all-atom additive force field for lipids: Validation on six lipid types. J Phys Chem B. 2010; 114:7830–7843. [PubMed: 20496934]
46. Martyna GJ, Tobias DJ, Klein ML. Constant pressure molecular dynamics algorithms. J Chem Phys. 1994; 101:4177–4189.
47. Feller SE, Zhang Y, Pastor RW, Brooks BR. Constant pressure molecular dynamics simulation: The Langevin piston method. J Chem Phys. 1995; 103:4613–4621.
48. Ryckaert JP, Ciccotti G, Berendsen HJC. Numerical integration of the Cartesian equations of motion of a system with constraints: Molecular dynamics of n-alkanes. J Comput Phys. 1997; 23:327–341.
49. Andersen HC. Rattle: A "velocity" version of the shake algorithm for molecular dynamics calculations. J Comput Phys. 1983; 52:24–34.
50. Darden T, York D, Pedersen LG. Particle mesh Ewald: An $N\log(N)$ method for Ewald sums in large systems. J Chem Phys. 1993; 98:10089–10092.
51. Comfurious P, Smeets E, Willems G, Bevers E, Zwaal R. Assembly of the prothrombinase complex on lipid vesicles depends on the stereochemical configuration of the polar headgroup of phosphatidylserine. Biochemistry. 1994; 33:10319–10324. [PubMed: 8068668]

Essentials

- Membrane-binding GLA domains of coagulation factors are essential for proper clot formation.
- Factor X (FX) is specific to phosphatidylserine (PS) lipids through unknown atomic-level interactions.
- Molecular dynamics simulations were used to develop the first membrane-bound model of FX-GLA.
- PS binding modes of FX-GLA were described, and potential PS-specific binding sites identified.

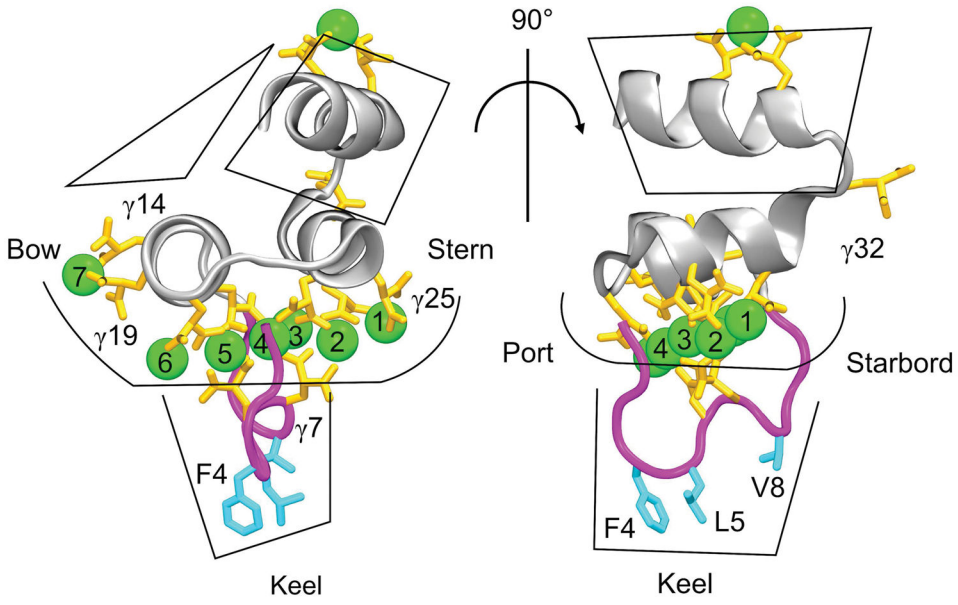

Figure 1.

The bovine FX GLA domain (FX-GLA) from protein databank structure 1IOD [27]. Significant features of the GLA domain are: 1) Ca^{2+} ions, shown as green balls, 2) specialized γ-carboxyglutamic acid residues, shown in orange, 3) the ω-loop, highlighted in magenta, and 4) the hydrophobic keel residues, high- lighted in blue. In order to refer to orientation of the GLA domain, we have appropriated the nautical terminology of “stern”, “bow”, “port” and “starboard” to refer to four sides of the protein.

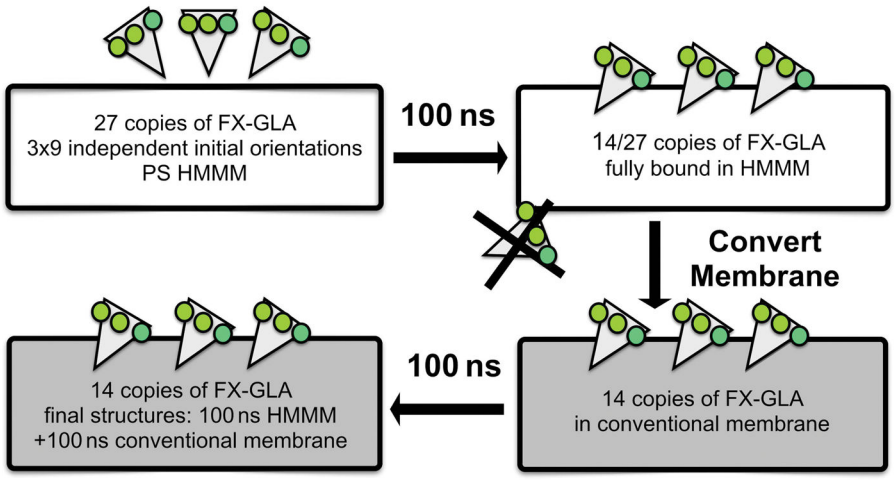

Figure 2.

Illustration of the simulation protocol for developing the FX-GLA membrane-bound model. After the initial 27 membrane binding simulations were run for 100 ns, the models with keel residues inserted below the level of the phosphate plane in the membrane (14 systems) were converted to conventional full-tailed membrane models and simulated each for an additional 100 ns.

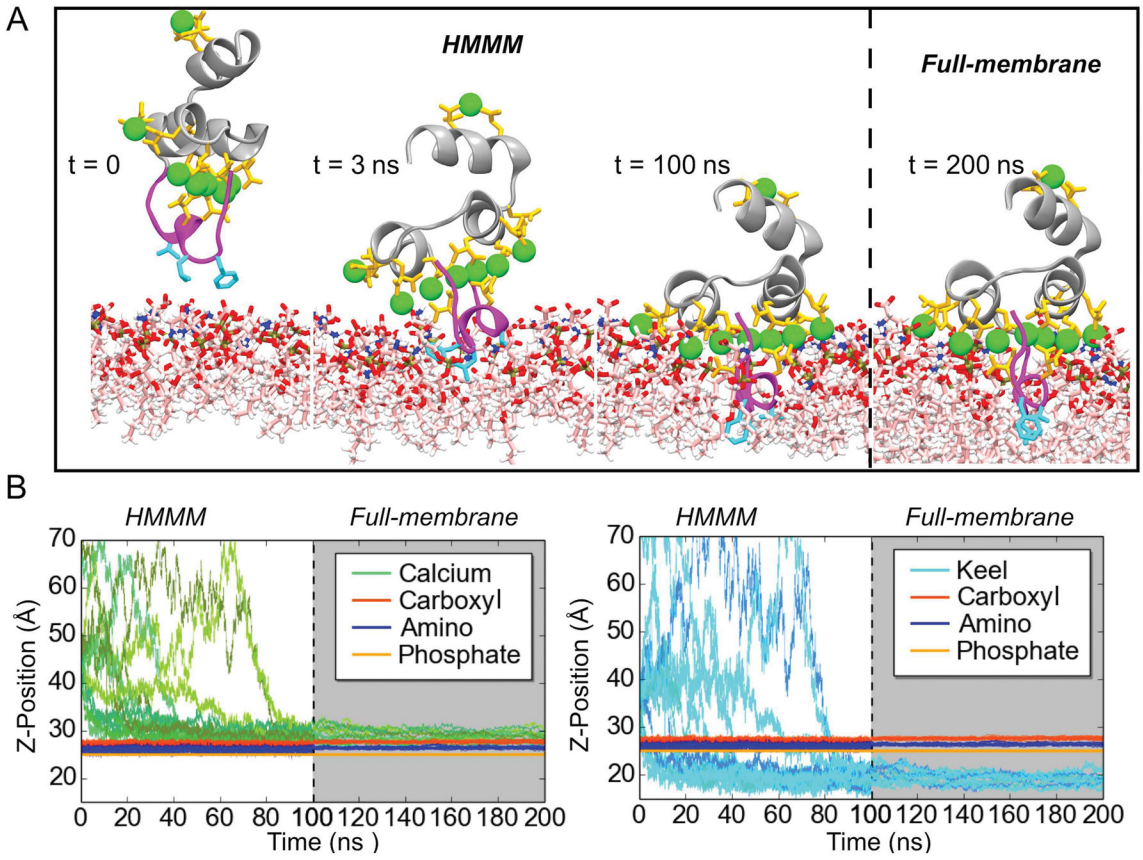

Figure 3.

Membrane binding and insertion of the FX-GLA domain. A) Binding of the FX-GLA domain at different time points along a representative trajectory. Until 100 ns (indicated by the dashed line), the domain is simulated in an HMMM membrane representation. Then, the membrane is converted to a full membrane. B) Relative positions on the z-axis of the COM of lipid phosphate, carboxyl and amino groups (both panels) and GLA domain residues (Ca^{2+} ions in left panel; backbone atoms of keel residues (PHE4, LEU5, and VAL8) in right panel). See Methods for atoms included in the phosphate, carboxyl, and amino groups. Grey background indicates portions of the trajectories with a full membrane. Data in this figure refer only to the 14 properly bound FX-GLA domain. Refer to Figure S3 for information on the 13 trajectories in which proper binding was not achieved within the time scale of the HMMM simulations (100 ns). See Methods for the definition of “proper” membrane binding.

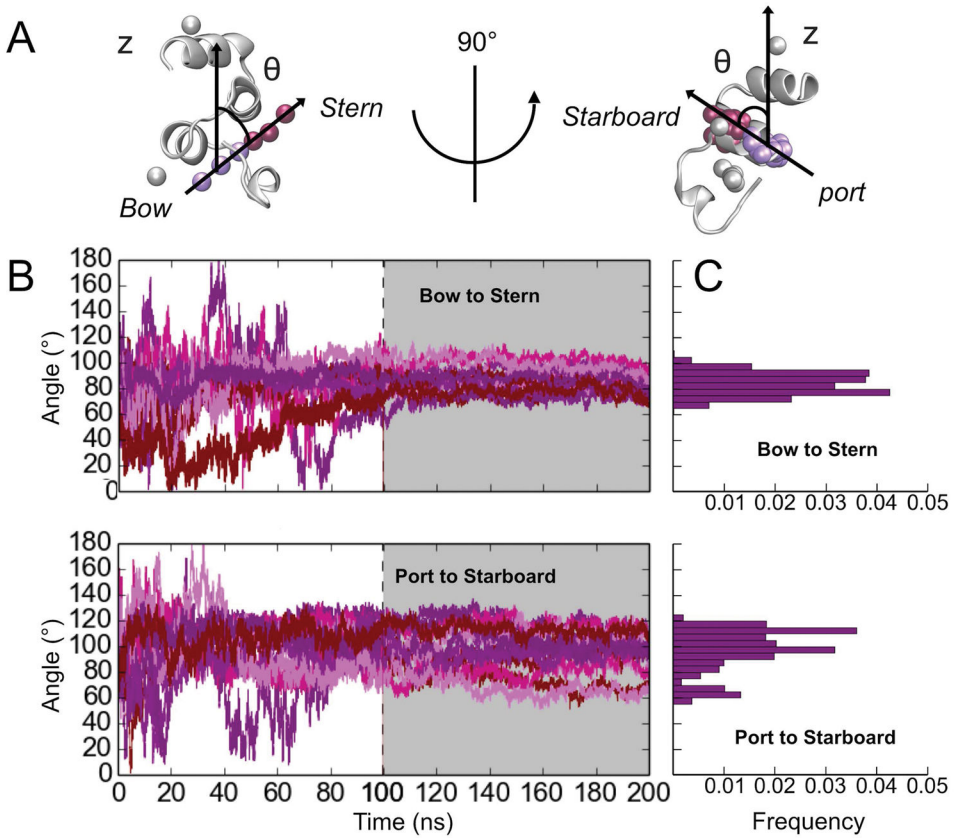

Figure 4.

FX-GLA orientation relative to the membrane normal. A) Illustration of the “bow-to-stern” and “port-to-starboard” angles to the membrane normal. Atoms used to define opposite ends the vectors are shown in violet and maroon balls. B) Data tracking the bow-to-stern (upper panel) and port-to-starboard (lower panel) angles for all 14 properly bound trajectories. The portion of each panel with a grey background is the 100 ns of simulations in full-membrane. C) Histogram of bow-to-stern (upper panel) and port-to-starboard (lower panel) angles calculated for the last 10 nanoseconds of simulations with full membranes. All 14 properly bound trajectories are included in the data.

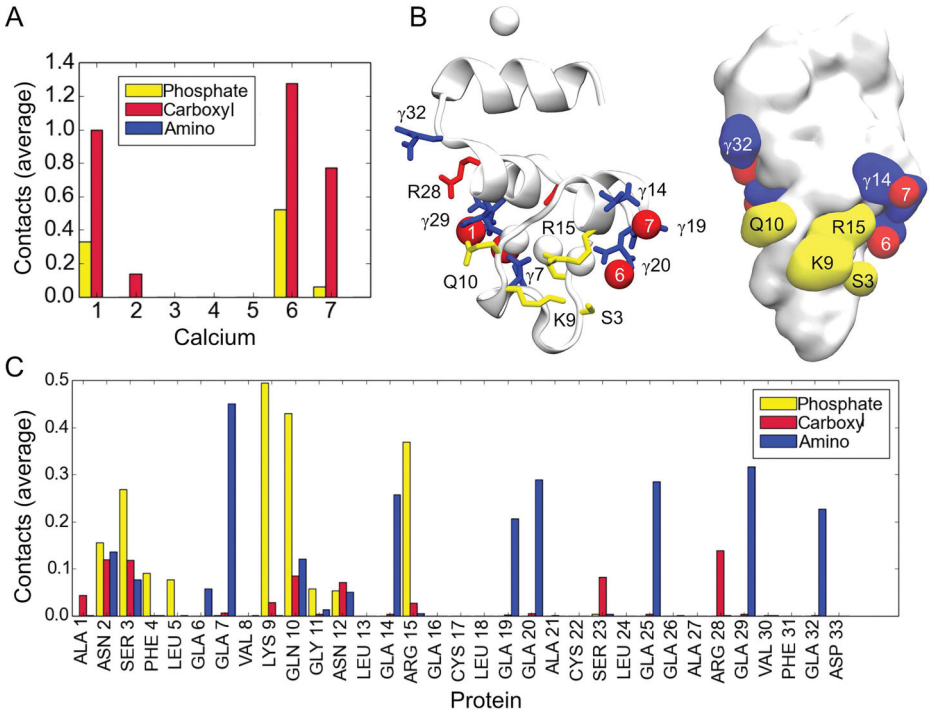

Figure 5.

Lipid contacts with the GLA domain. A) Histogram of average contacts between Ca^{2+} ions on the GLA domain and carboxyl and phosphate groups in PS lipids. B) Illustration of the FX-GLA domain indicating protein residue and Ca^{2+} ion numbering, along with the charged group with majority of contacts to the residue. Blue indicates a lipid amino interaction, red indicates a lipid carboxyl interaction, and yellow indicates a lipid phosphate interaction. Only average contact numbers 0.1 or greater are illustrated with a color code. C) Histogram of protein residue contacts to lipid charged groups. Average contact values are calculated across all 14 trajectories for the entire 100 ns of the full-membrane simulations. Refer to Methods for details on contact calculation.

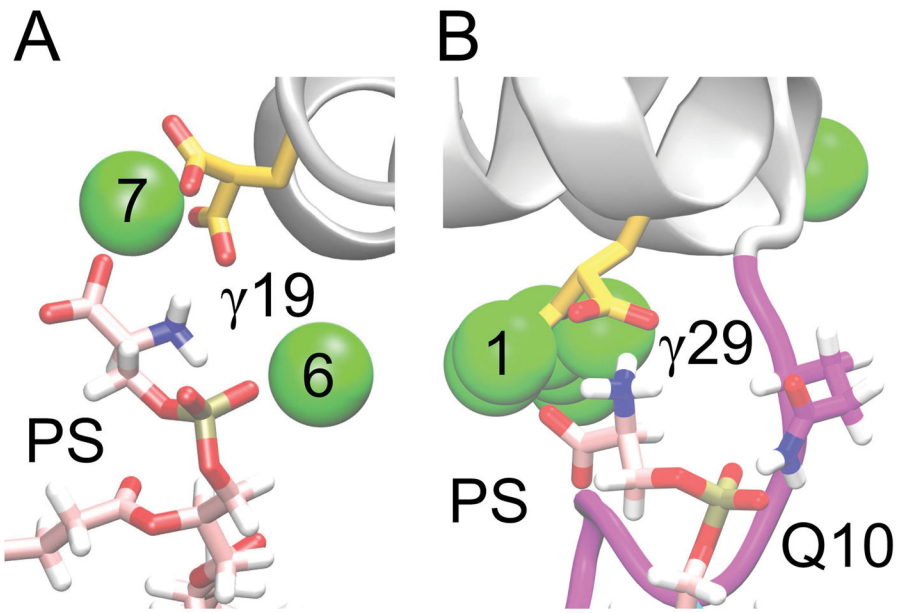

Figure 6.

Putative PS binding sites. We present here the two putative PS binding sites which are proposed based on our lipid contact frequency calculations (Figure 5). A) Putative site 1, including interactions between PS carboxyl and Ca-7, between PS amino and GLA19, and between PS phosphate and Ca-6. B) Putative site 2, including interactions between PS carboxyl and Ca-1, between PS amino and GLA29, and between PS phosphate and GLN10.

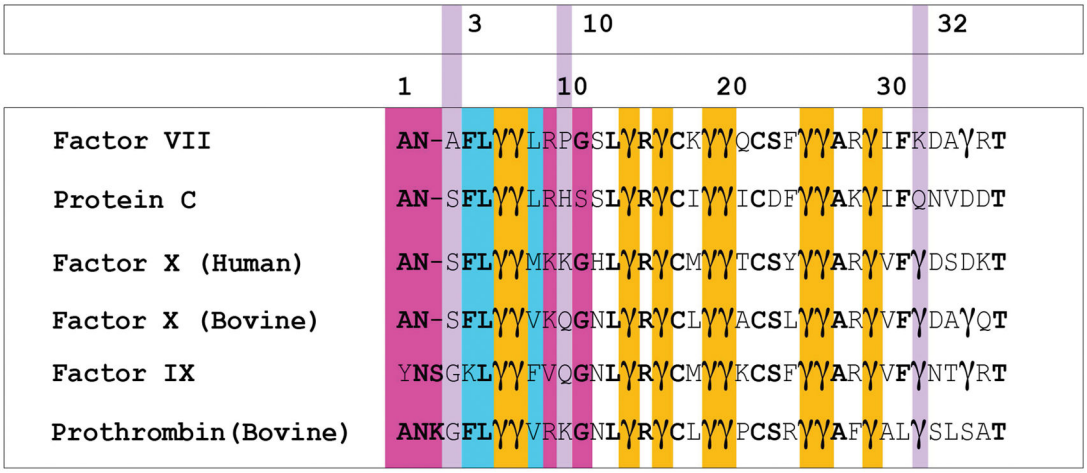

Figure 7.

The BLAST sequence alignment of coagulation factor GLA domains discussed in this study, namely: phosphatidic-acid (PA) specific domains factor VII and protein C; and PS specific domains factor X (human), factor X (bovine), factor IX, prothrombin (bovine). Unless specified otherwise, all sequences are human in origin. Cyan indicates residues of the keel (residues 4, 5, and 8). Gold indicates GLA-residues whose positions are conserved among all GLA domains. Violet is used to indicate location of residues involved in membrane interactions which differ between FX-GLA and FVII-GLA, and the FX-GLA sequence number for these residues is reported in the top row of numbers. At sequence position 3, SER3 in FX-GLA is replaced by ALA3 in FVII-GLA. At sequence position 10, which was found to participate interactions with lipid phosphate groups, the PA-specific domains carry hydrophobic residues, while the PS-specific domains contain residues capable of interactions with anionic lipids. At sequence position 32, PA-specific domains contain positively charged residues, while the PS-specific domains contain negatively charged residues. The bottom row of numbers marks every 10^{th} sequence position in the alignment. Magenta is used to highlight residues in the ω-loop, residues 1–11, which were not otherwise highlighted.

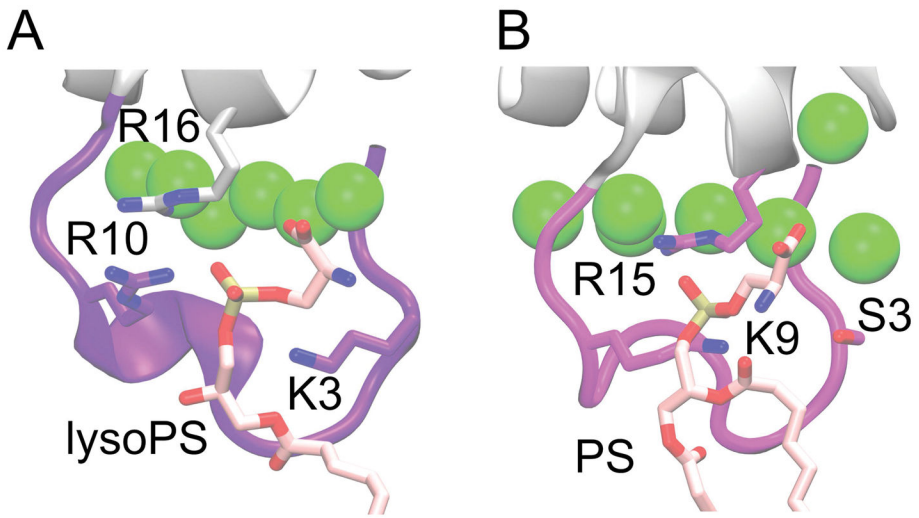

Figure 8.

Comparison of phosphate binding site for A) prothrombin-GLA co-crystallized with a single lysoPS (PDB 1NL2) [8], and B) FX-GLA bound to PS from one of our full-membrane simulations. Binding of PS is similar in both cases, with the equivalent starboard face residues (ARG10 and ARG16 on prothrombin-GLA, LYS9 and ARG15 on FX-GLA) interacting with the phosphate group. SER3 in FX-GLA does not interact with the phosphate, however, unlike LYS3 in the prothrombin structure.

Table 1

Protein-lipid contacts. Average contact values≥0.05 reported, rounded to two decimal places. The standard deviation is reported in parentheses.

Residue	Carboxyl	Phosphate	Amino
ASN 2	0.12(0.08)	0.16(0.08)	0.14(0.11)
SER 3	0.12(0.07)	0.27(0.11)	0.08(0.08)
PHE 4		0.09(0.07)	
LEU 5		0.08(0.06)	
GLA 6			0.06(0.04)
GLA 7			0.5(0.09)
LYS 9		0.50(0.12)	
GLN 10	0.09(0.09)	0.43(0.15)	0.12(0.12)
GLY 11		0.06(0.05)	
ASN 12	0.07(0.07)	0.05(0.06)	
GLA 14			0.26(0.07)
ARG 15		0.37(0.10)	
GLA 19			0.21(0.06)
GLA 20			0.29(0.08)
SER 23	0.08(0.05)		
GLA 25			0.29(0.07)
ARG 28	0.14(0.06)		
GLA 29			0.32(0.08)
GLA 32			0.23(0.08)

Table 2

Ca^{2+}-Lipid Contacts. Average contact values rounded to two decimal places. The standard deviation is reported in brackets.

Ca^{2+}	Carboxyl	Phosphate
1	1.00(0.14)	0.33(0.08)
2	0.14(0.04)	0.00
3	0.00	0.00
4	0.00	0.00
5	0.00	0.00
6	1.23(0.19)	0.52(0.10)
7	0.77(0.10)	0.06(0.03)